Analytica Chimica Acta 1207 (2022) 339742

Contents lists available at ScienceDirect

Analytica Chimica Acta

journal homepage: www.elsevier.com/locate/aca

Rapid nanomolar detection of methamphetamine in biofluids via a reagentless electrochemical aptamer-based biosensor

Yu Xie , Shenghong Wu , Zhimin Chen , Jinzhi Jiang **, Jianjun Sun *

Ministry of Education Key Laboratory for Analytical Science of Food Safety and Biology, College of Chemistry, Fuzhou University, Fuzhou, 350116, China

HIGHLIGHTS

- A simple, cost-effective and reagentless electrochemical aptamer-based (EAB) sensor was constructed.
- The sensor enabled sensitive detection of methamphetamine (MAMP) with a nanomolar level.
- The recovery window of the MAMP sensor in bio-sample was far below the clinical range.
- The method would be hopefully used for preliminary screening of drugged driving.

GRAPHICAL ABSTRACT

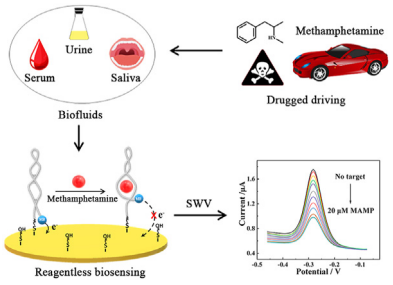

ARTICLE INFO

Article history:
Received 28 January 2022
Received in revised form
4 March 2022
Accepted 17 March 2022
Available online 19 March 2022

Keywords:
Methamphetamine
Aptamer
Electrochemical sensor
Reagentless
Nanomolar detection
Biofluids

ABSTRACT

The availability of sensing platforms able to rapidly measure abused drugs directly in biological fluids in a single step would allow performing drugged driving screening on the site. The achievement of this goal is extremely important for preventing and controlling drug abuse and crime incidence. Motived by this, we constructed a simple, cost-effective and reagentless electrochemical aptamer-based (EAB) sensor with methamphetamine (MAMP) as the target molecule. This EAB sensor produced a nanomolar level of detection accuracy in unprocessed or minimally processed bio-samples. Specifically, circular dichroic spectrum was used to confirm that the truncated aptamer from the original sequence would undergo large binding-induced conformational changes. We then engineered the aptamer to work in the EAB platform and the resulting sensor enabled sensitive and specific detection of MAMP with the detection limit of 30 nM in undiluted serum, 50 nM in undiluted urine and 20 nM in 50% saliva. The sensor has good recovery rate, implying this method has good reliability and repeatability. The detection limit is far below the clinical detection threshold, it would be hopefully used for preliminary screening of drugged driving in real world.

1. Introduction

Methamphetamine (MAMP) is the most widely abused central nervous system stimulant and is reported to be the second most commonly used class of illicit drugs worldwide with a tendency toward growth [1,2]. Drug abuse has caused serious harm to people and society such as the loss of life and health of abusers, increased treatment costs, and higher crime incidence [3,4]. Drug on-site detection is of great significance to combating drug crimes and stopping drug transactions [5,6]. A rapid and cost-effective method for detecting drugs in body fluids was an important reference basis for the law enforcement of field trials [7]. For example, the

* Corresponding author.
** Corresponding author.
E-mail addresses: jiangjinzhi@fzu.edu.cn (J. Jiang), jjsun@fzu.edu.cn (J. Sun).

https://doi.org/10.1016/j.aca.2022.339742
0003-2670/

shortened sleep time and subsequent fatigue caused by MAMP are important risk factors for motor vehicle collisions [8]. It is unsafe to drive when the MAMP concentration in blood is higher than the threshold of 168 nM [8,9]. At present, various methods have been developed for detection of MAMP, such as gas chromatography-mass spectrometry (GC-MS) [10], high-performance liquid chromatography (HPLC) [11], immunoassays [12,13], surface-enhanced Raman spectroscopy (SERS) [14,15], ion mobility spectrometry [16], fluorescence [17] and electrochemical method [18]. Among these, electrochemical technology has aroused great interest due to the advantages of high sensitivity, low cost, simple equipment, and easy miniaturization [19].

The electrochemical aptamer-based (EAB) sensor platform, which operates via the target binding-induced folding of DNA and RNA aptamers was widely used for the detection of small molecule targets such as metabolites, drugs, and environmental toxins [20]. This technology harness redox-reporter-modified, structure-switching aptamer as the sensing element [21]. The target-induced conformation change of the aptamer alters the electron transfer dynamics between the reporters and the electrode surface in a monotonically related manner to the target concentration [22,23]. It is still challenging to design MAMP sensors with low cost, simple aptamer modification and high sensitivity. Ideally, an aptamer electrochemical sensor requires that the aptamer undergoes a large conformational change when it binds to the target and has a strong affinity to the target.

Aptamer truncation has been proved to be an effective means to reduce cost and enhance target affinity and selectivity [24]. Gao et al. developed a novel fluorescently labeled aptamer for the detection of gliotoxin based on optimized truncated aptamer [25]. He et al. screened high-affinity aptamer for methotrexate (MTX) through SELEX and aptamer truncation, and used them for the highly sensitive detection of MTX [26]. Interestingly, Ebrahimi et al. established a specific ssDNA aptamer that can recognize MAMP by SELEX technology [27]. However, primer chains are required in the SELEX process, which leads to very long aptamer sequences. The MAMP aptamer composed of 84 bases is costly to synthesize, and may also complicate the rational design of biosensors for MAMP detection [28]. To overcome this obstacle, we removed the primer chain and chose the 40-base sequence with a good affinity for MAMP. And then, one and two bases were truncated at both ends of the sequence to obtain 36 nt and 38 nt aptamers. The 38 nt aptamer was finally found to show stronger structure-switching functionality to MAMP compared to the 36 nt and 40 nt aptamer.

In this work, we used circular dichroism to screen out the aptamer with the largest target-induced conformational change and modified it with methylene blue on one end and a thiol group on the other, which were immobilized on the gold electrode surface to construct an EAB sensor for efficient, rapid and selective detection of MAMP. The design and sensing mechanisms are shown in Scheme 1. Upon MAMP binding, the aptamer underwent a conformation change and brought methylene blue away from the electrode surface, leading to decreases of electric current, thereby indirectly measuring the molecular concentration. Upon introduction of the target, binding-induced steric hindrance quantitatively reduces the efficiency of electron transfer of a distal-end redox label leading to the rapid signal change within 60 s. Furthermore, because the redox-active reporter is covalently linked to the nucleic acid aptamer, this allows sensor function without the addition of exogenous reagents [29]. To the best of our knowledge, this is the first reagentless EAB sensor capable of measuring MAMP based on the "signal off" mechanism. The structure-switching sensor was unveiled for the specific and rapid sensing of MAMP with good analytical performances, achieving the nanomolar detection of MAMP in biofluids such as undiluted serum, urine and 50% saliva, with detection limits of 30 nM, 50 nM and 20 nM, respectively, which were far below the physiological concentration threshold. These results illustrated that the developed assay has significant potential and offered an alternative to the traditional analytical methods to achieve the sensitive and efficient detection of MAMP.

2. Experimental section

2.1. Materials

Methylamphetamine, cocaine, ketamine and morphine (1 ppm) were received from Xiamen Pushi nanotechnology Co., Ltd (Fujian, China). Tris(2-carboxyethyl) phosphine (TCEP), 6-mercapto-1-hexanol (MCH) and trizma preset crystals (pH 7.4) were obtained from Sigma-Aldrich. Fetal calf serum was bought from Tianhang

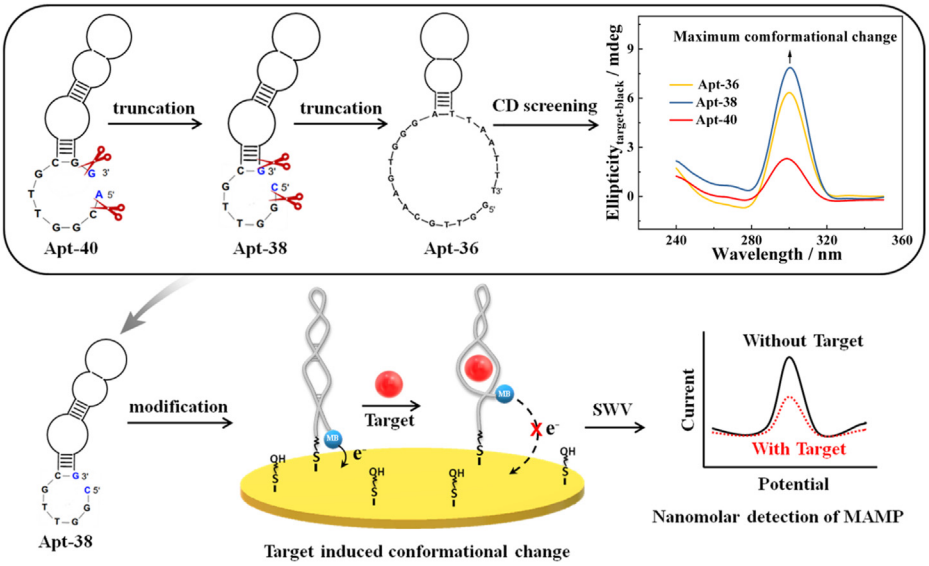

Scheme 1. Schematic diagram of EAB sensors and the detection process. The detection of MAMP relies on MAMP-binding changes to the steric hindrance of signaling aptamer probes, resulting in a decrease in measured electrochemical signal.

Biotechnology Co., Ltd (Zhejiang, China).

DNA oligonucleotides were synthesized and further purified by Sangon Biotechnology Co., Ltd. (Shanghai, China), 10 mM Tris-HCl buffer was added to it to a final concentration of 100 μM, and stored at −20 °C for use. The aptamer sequences we used are as follows:

Apt-40: 5′-ACGGTTGCAAGTGGGACTCTGGTAGGCTGGGTTAATTTGG-3′
Apt-38: 5′-CGGTTGCAAGTGGGACTCTGGTAGGCTGGGTTAATTTG-3′
Apt-36: 5′-GGTTGCAAGTGGGACTCTGGTAGGCTGGGTTAATTT-3′

2.2. Circular dichroism (CD)

The 20 mM Tris buffer (pH 7.4) containing 200 mM NaCl and 5 mM $MgCl_2$ was used for the experiments. The aptamer Apt-40, Apt-38 and Apt-36 (final concentration 6.0 μM) were added to binding buffer, respectively, heated at 95 °C for 10 min, and then immediately cooled down on the ice. Different concentrations of MAMP were added to the aptamer solution and incubated overnight at room temperature. The CD spectrums were recorded from 360 to 200 nm on a MOS-450 spectropolarimeter (BIO-LOGIC Company, France). The data gathered were the average of four times scans with the scan rate of 100 nm/min subtracting the spectra of the buffer.

2.3. Sensor fabrication on gold-disk electrodes

A 38-base aptamer sequence was finally used for the EAB sensor, 3′ end of this aptamer was labeled with methylene blue (MB) and its 5′ end was modified with a six-carbon thiol (SH—C6), which is listed below: 5′—SH—C6-CGGTTGCAAGTGGGACTCTGGTAGGCTGGGTTAATTTGG-MB-3'. Before sensor fabrication, 2 mm diameter gold disk electrodes were polished with 1 μm and 0.05 μm diamond slurry. And then the electrodes were sonicated in ethanol and water for about 6 min, respectively. The electrodes were cleaned electrochemically by cyclic voltammetry (CV) for 500 cycles between −0.35 and −1.35 V (vs. Ag/AgCl) at scan rate of 2 V s^{-1} in 0.5 M NaOH solution. Then the electrodes were placed in 0.5 M H_2SO_4 to perform CV scanning between 0.4 V and 1.6 V at 4 V s^{-1}, followed by scanning at 0.1 V s^{-1} for 20 cycles. The labeled aptamer was first reduced by mixing 1 μL of the aptamer solution (100 μM) and 9 μL of 100 mM TCEP solution at room temperature for 2 h. Then PBS buffer (10 mM phosphate, 1 M NaCl, 1 mM $MgCl_2$, pH 7.0) was added to it and diluted to obtain 200 nM of aptamer solution. The freshly cleaned electrodes were incubated in the aptamer solution for 1 h, followed by washing with deionized water, and then backfilled using 3 mM MCH solution at room temperature for 1 h. Finally, the sealed electrodes were washed with deionized water and then incubated in 20 mM tris buffer overnight.

2.4. Electrochemical experiments

Electrochemical data were collected using CHI 1030 electrochemical workstation (CH Instruments, China). Three-electrode system including a Au working electrode (Jinhuice.com, Nanjing, China), a Ag/AgCl (saturated KCl) reference electrode and a platinum wire counter electrode. Electrochemical impedance spectrometry (EIS) was carried out in 0.1 M KCl solution containing 5.0 mM $[Fe(CN)_6]^{3-/4-}$ in a frequency range from 0.1 Hz to 10 kHz with 5 mV as the amplitude at room temperature. Square wave voltammetry (SWV) is exquisitely sensitive to electrode reaction rates. It's commonly used to interrogate EAB sensor surfaces. Changes in SWV frequency also offer the potential to tune the sensitivity of EAB sensor [29]. SWV was acquired with 1 mV potential step and an amplitude of 25 mV at the frequency of 200 Hz. The sensor was immersed in the electrochemical cell which contains the working buffer (20 mM Tris buffer, 200 mM NaCl, 5 mM $MgCl_2$, pH 7.4). The binding curves were conducted by using the MAMP concentrations of 0.03, 0.05, 0.1, 0.25, 0.5, 1, 3, 5, 10 and 20 μM. The electrodes were used to detect MAMP in working buffer, 50% saliva, serum and urine, respectively. The limit of detection (LOD) is determined based on a signal-to-noise ratio (S/N) of 3 [30]. Scheme 1 illustrates the mechanism of the MAMP aptasensor based on signal suppression with DNA superstructures. Signal suppression (*SS*) was calculated using the following equation:

$$\text{Signal Suppression } (SS) = [(I_0 - I)/ I_0] \times 100\%$$

Where I_0 and I are the SWV baseline-subtracted peak currents in the absence and presence of MAMP under the frequency of 200 Hz, respectively.

3. Results and discussion

3.1. Secondary structure prediction

To improve the performance of the sensor, we redesigned the original aptamer and destabilized its secondary structure by truncating the bases at both ends of the aptamer. The truncated aptamers contained 36 and 38 bases, respectively, and their secondary structure was predicted by NUPAK (Fig. 1) [31]. The results showed that this strategy decreased the stability of the aptamer from −2.17 kJ mol^{-1} (Apt-40) to −1.2 kJ mol^{-1} (Apt-36). The aptamer formed a more open or unfolded state due to this destabilization, resulting in larger target-induced conformational changes, thus showing greater current signal changes [32].

3.2. Circular dichroism

To find the optimally destabilized variant, conformational characterization of 36 nt, 38 nt and 40 nt MAMP aptamer was carried out. The CD spectra of MAMP aptamer in the absence and presence of different concentrations of MAMP were recorded and the results were shown in Fig. 2 (A-C). As the target concentration increased from 0 μM to 100 μM, the peak intensities of different aptamers at 290 nm changed, indicating that the structure of the MAMP aptamer was induced to change after ligand binding [33]. The peak at 290 nm in the CD spectrum blue-shifted upon the addition of MAMP (Fig. 2B), and the intensity increased accordingly because the addition of MAMP likely stabilized the secondary structure of the Apt-38 aptamer [8,28] From Fig. 2D, it can be seen that the peak intensity change of the Apt-38 is larger than that of Apt-36 and Apt-40. This implied that the conformational change of the Apt-38 is larger than the change of the other aptamers. Therefore, the Apt-38 aptamer was used for EAB sensing in subsequent experiments due to its stronger structure-switching functionality. The 3′ end of this aptamer was labeled with methylene blue and the 5' end was labeled with six-carbon thiol, which was immobilized on a gold electrode and used to construct an EAB sensor to detect MAMP.

3.3. Electrochemical impedance spectroscopy (EIS)

EIS was performed to characterize the charge transfer resistance (R_{ct}) of the electrode interface [34–36]. A redox probe ($Fe(CN)_6^{3-/4-}$) is usually used that its charge transfer ability changes due to steric or electrostatic blocking of a functionalized electrode [37].

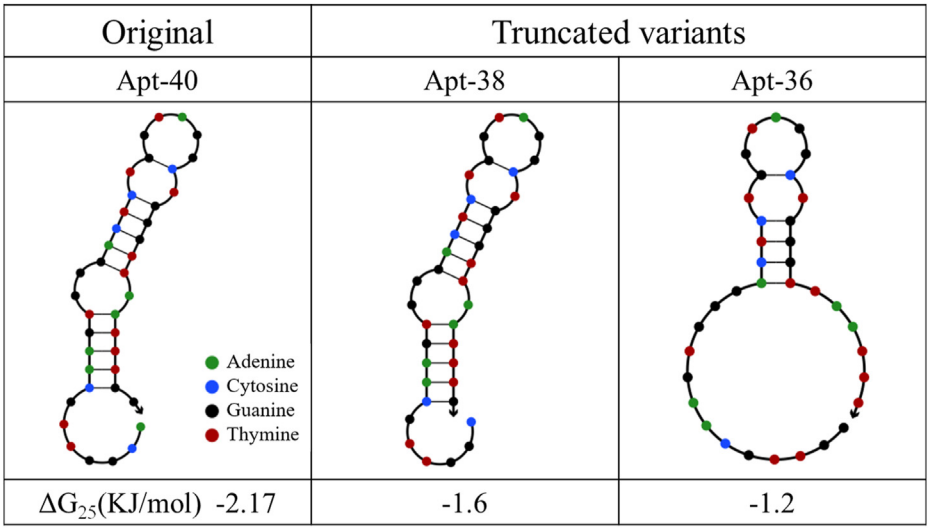

Fig. 1. Secondary structure prediction of Apt-36, Apt-38, and Apt-40 aptamer.

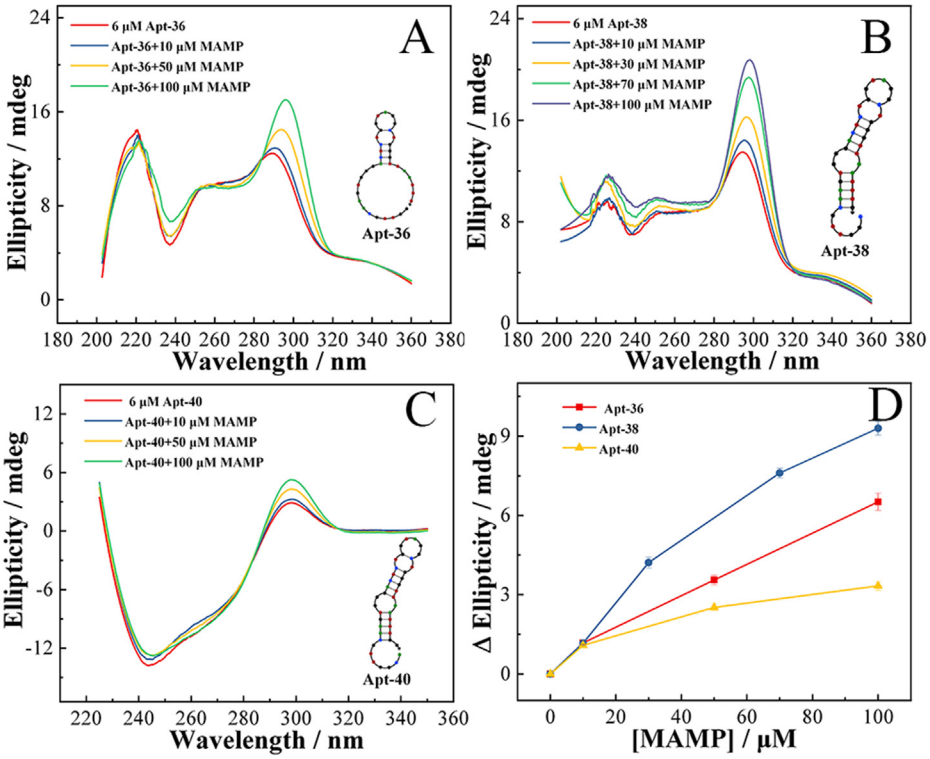

Fig. 2. The circular dichroism spectrum of the 6 μM Apt-36 (A), Apt-38 (B), and Apt-40 (C) aptamer with different MAMP concentrations in 20 mM Trisbuffer (pH 7.4) containing 200 mM NaCl and 0.05 mM $MgCl_2$. (D) Peak intensity changes of the circular dichroism spectrum at 290 nm with the increasing concentration of MAMP.

Fig. 3 displayed the Nyquist plots. The bare Au electrode exhibited a smaller R_{ct} (curve a), indicating a fast electron transfer process of the redox couple $[Fe(CN)_6]^{3-/4-}$ [38]. A significant semicircle with enhanced electron transfer resistance was observed after the modification of aptamer on the electrode surface (curve b). After the modification of MCH on Au/Apt, the R_{ct} increased obviously, indicating restricted charge transfer (curve c) [39]. R_{ct} continued to increase when the Au/Apt/MCH was incubated with 1 μM (curve d) and then with 5 μM (curve e) MAMP successively. This means that with the addition of MAMP, more targets are bound to aptamers, resulting in significant changes in the conformation of aptamers.

3.4. The optimum frequency

The frequency of SWV analysis has been regarded as an important fact to define the sensitivity of the aptamer [40]. The frequency of the voltammetric measurements can be tuned to preferentially enhance the signal associated with the target-bound conformations of the probe [41]. We collected the SWV response with and without the presence of 5 μM MAMP over frequencies varying from 5 to 400 Hz. As the frequency increased, the SWV response current increased (Fig. 4A). At a certain frequency, the response current was suppressed after the target was added,

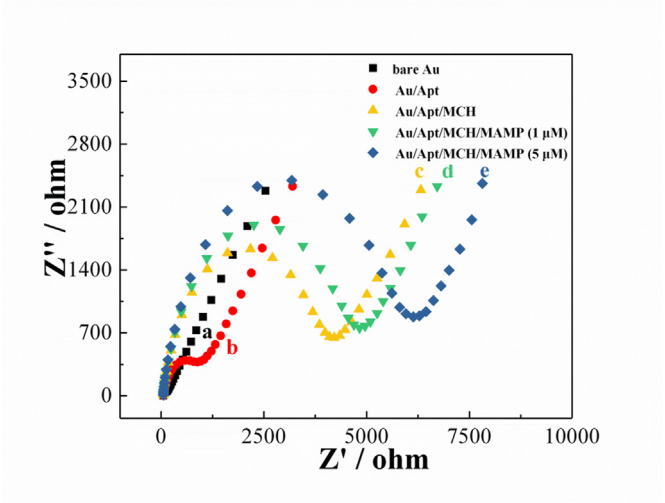

Fig. 3. Nyquist plot of different electrodes: bare Au electrode (curve a), the Apt-38 aptamer modified Au electrode (Au/Apt, curve b), Au/Apt/MCH electrode (curve c) without and with the incubation of 1 μM (curve d) and 5 μM (curve e) MAMP. EIS was carried out in 0.1 M KCl solution containing 5.0 mM $[Fe(CN)_6]^{3-/4-}$ in a frequency range from 0.1 Hz to 10 kHz with 5 mV as the amplitude at room temperature.

indicating that the sensor was a signal-off EAB sensor. On hybridization, the distance between the label and the electrode changed significantly, resulting in large and easily measurable signal changes [42]. Fig. 4B shows that the signal change reached a relatively large value within the frequency range from 200 to 400 Hz, so subsequent SWV tests were carried out at 200 Hz.

3.5. The detection of MAMP in biofluids

To verify the applicability of this method, we fabricated EAB sensors using the gold electrode modified with a thiol-methylene blue-labeled aptamer, which was applied to the detection of MAMP in the working buffer and different biofluids including undiluted serum, undiluted urine and 50% saliva. Typical SWVs with MB reduction peak were shown and the sensor produced decreasing current with increasing concentrations of MAMP (Fig. 5A–D). The target dose-response curve (Fig. 5E–H) was fitted by the Hill equation (equation (1)) to obtain the parameters of the MAMP sensor (Table 1) [43].

$$SS = r_{min} + (r_{max} - r_{min})\frac{[target]^n}{k_d^n + [target]^n} \quad (1)$$

Wherein n is the Hill coefficient, *SS* means the signal suppression; r_{min} and r_{max} represent the minimum and maximum values of the suppression signal. And k_d is the midpoint of the binding curve for the sensor class. Equation (1) was recast to obtain the target concentration (equation (2)):

$$[Target] = k_d \sqrt[n]{\frac{SS - r_{min}}{r_{max} - SS}} \quad (2)$$

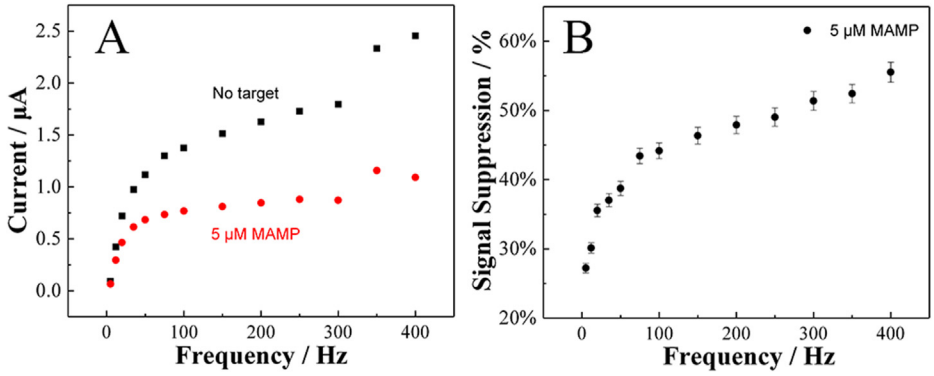

Fig. 4. (A) The frequency-dependent of SWV current responses for the EAB sensor with and without 5 μM MAMP in working buffer. (B) Signal Suppression of 5 μM MAMP at different frequencies. Frequency: 5, 12, 20, 35, 50, 75, 100, 150, 200, 250, 300, 350, 400 Hz.

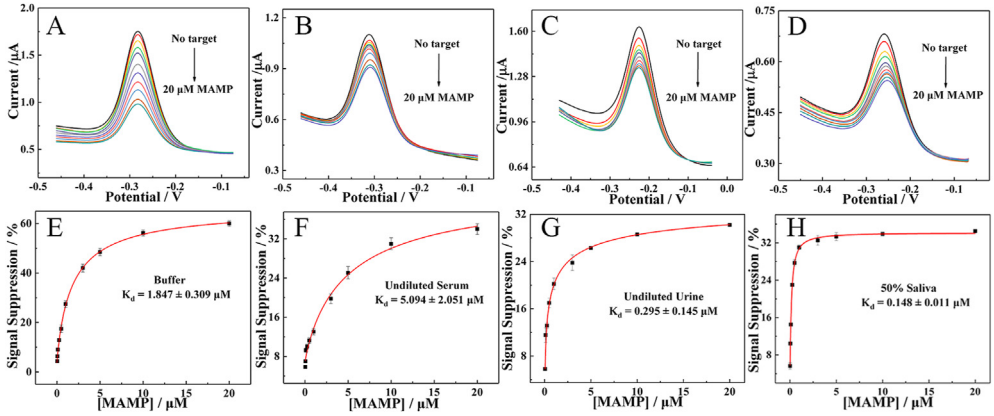

Fig. 5. SWVs of the MAMP sensor in working buffer (A), undiluted serum (B), undiluted urine (C) or 50% saliva (D) and the calibration curves of the MAMP sensor in working buffer (E), undiluted serum (F), undiluted urine (G) or 50% saliva (H). Error bars represent standard deviation from three experiments.

Table 1
The parameters r_{min}, r_{max}, $k_{1/2}$, n for the EAB sensor in working buffer, undiluted serum, undiluted urine and 50% saliva.

Parameters	Buffer	Serum	Urine	Saliva
$\mathbf{r_{min}}$	3.762 ± 0.879	6.816 ± 0.953	−8.173 ± 5.898	2.686 ± 1.023
$\mathbf{r_{max}}$	66.89 ± 2.056	42.84 ± 5.908	35.86 ± 1.768	34.169 ± 0.292
$\mathbf{K_{1/2}}$	1.846 ± 0.161	5.094 ± 2.051	0.295 ± 0.145	0.148 ± 0.011
n	0.904 ± 0.064	0.886 ± 0.191	0.448 ± 0.082	1.107 ± 0.073

From those data, the EAB sensor was able to detect MAMP with a limit of detection (LOD) of 30 nM in working buffer (Fig. 5A), and the detection range was from 30 nM to 20 μM. The dissociation constant (K_d) was 1.846 ± 0.161 μM (Table 1).

The feasibility of this strategy was further validated by generating the calibration curve by adding different concentrations of MAMP to the biofluids. The SWV signal decreased as the MAMP concentration increased with the range from 30 nM to 20 μM and a measurable detection limit of 30 nM in undiluted serum (Fig. 5B). The K_d value of the MAMP aptasensor in undiluted serum was 5.094 ± 2.051 μM (Table 1). The lowest measured amount of MAMP in serum was sufficient to detect the typical MAMP concentration of the impaired driver, which was below the concentration threshold of 168 nM [8]. Moreover, we were able to quantify the MAMP concentration in the range of 0.05–20 μM in undiluted urine (Fig. 5C). The LOD of MAMP in undiluted urine was 50 nM, which was far below the detection threshold in urine (200–671 nM) [9]. And the sensor was also able to detect the MAMP in 50% saliva over the range of 0.02–20 μM (Fig. 5D) with LOD of 20 nM. Table 2 shows previously reported assays for MAMP, the detection range and LOD of this EAB is comparable to several other assays, and requires no exogenous reagents or modified materials [44–52]. Those results indicated that this reagentless approach achieved nanomolar detection of MAMP in biofluids, which provided a rapid and useful tool for the police to detect drugs on the spot quickly and conveniently.

Table 2
Comparison of analytical performance of different MAMP sensors.

Detection Method	Modifier	Range (μM)	LOD (nM)	Reference
Voltammetric (DPV)	PGE	74–54 × 10^3	50	44
Voltammetric (DPV)	GCE/EDOT-BTDA-Pala /Antibody/MAMP	71.31–713.1	93.2	45
Impedimetric	AuNPs/MWCNTs-Nf/SPE	1.15 × 10^{-3} −2.69 × 10^{-2}	0.3	46
Impedimetric	Antibody-colloidal Au	0–1.675	670	47
Electrochemiluminescence	GCE/RuSiNPs-Nafion	0.1–10	26	48
Fluorimetric	Anti-MAMP-CdS QDs	0.14–17.85	42.78	49
Fluorimetric	SiO_2@QDs@ms-MIPs	5–250	1.6 × 10^3	50
SPR	AuNPs-BSA-Anti-MAMP	7.13 × 10^{-3}-7.13	1.14	51
Colorimetric	Salt/Aptamer/AuNPs	2–10	820	52
EAB sensor	Apt-38-MB	0.02–20	20	This work

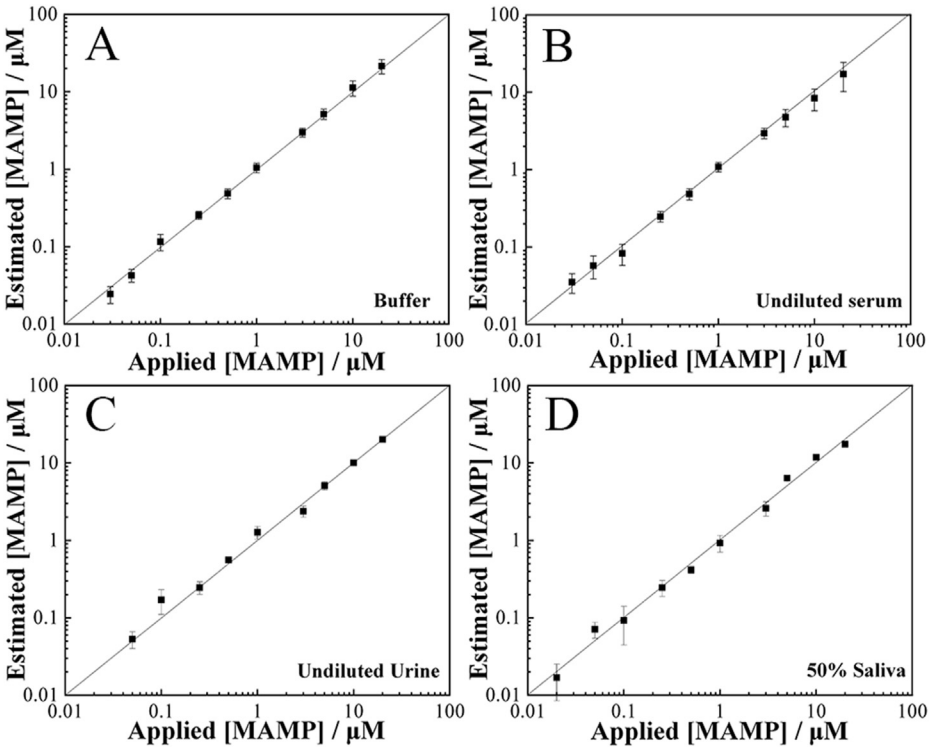

Fig. 6. Recovery tests of MAMP sensors interrogated in the working buffer (A) undiluted serum (B) undiluted urine (C) and 50% saliva (D), respectively. We achieved excellent accuracy with good recoveries both in working buffer (84.53–115.8%), undiluted serum (82.76–117.47%), undiluted urine (79.10%–127.15%) and 50% saliva (83.50%–127.03%).

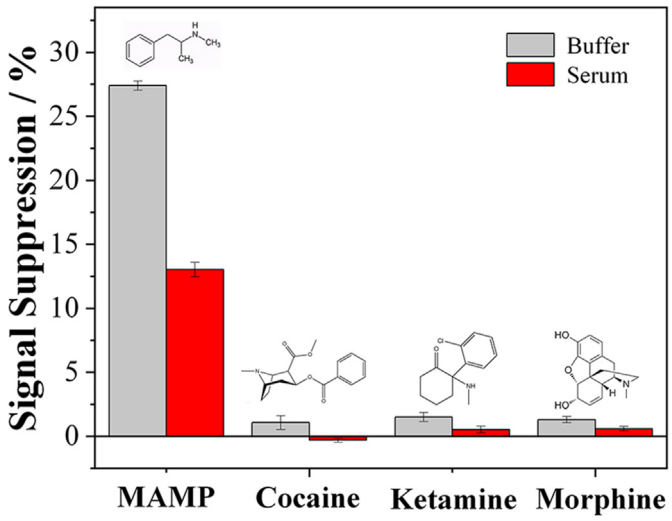

Fig. 7. Selectivity of the MAMP sensor in working buffer and undiluted serum. The bar plot shows signal suppressions produced by cocaine (10 μM), ketamine (10 μM), and morphine (10 μM) and their cross-reactivity relative to 1 μM MAMP. Inset shows structures of MAMP, cocaine, ketamine and morphine. Error bars represent the standard deviations in three individual experiments.

3.6. The recovery tests

To illustrate the effectiveness of the approach, we applied the parameters (Table 1) to a new set of sensors in working buffer and biofluids for recovery tests. The estimated concentrations were fell within the detection range of the respective calibration curves generated with aptamer-modified electrodes (Fig. 6). Good recoveries were obtained within the acceptable range in both working buffer (84.53–115.8%), undiluted serum (82.76–117.47%), undiluted urine (79.10%–127.15%) and 50% saliva (83.50%–127.03%). The results illustrated the good accuracy of the EAB sensor and proved that the sensor has practical application feasibility in biological environment.

3.7. The selectivity

We tested the selectivity of the sensor with three interfering drugs, cocaine, ketamine and morphine. The changes of suppression signals after the addition of 1 μM MAMP, 10 μM cocaine, 10 μM ketamine and 10 μM morphine were shown in Fig. 7. We found those interfering drugs exhibited low levels of signal suppression which was below 5%. These results indicated that the binding affinity of MAMP to Apt-38 was much stronger than that to all other illicit drugs, rendering the biosensor with high specificity towards MAMP.

4. Conclusion

In summary, we have developed a simple, fast and reagentless E-AB sensor for detection of MAMP. Especially, we demonstrated for the first time the use of truncated aptamer sequences with good affinities for the detection of MAMP. Through CD characterization, the aptamer underwent a big a large target- induced conformational transition, which was finally used to construct the EAB sensor. The sensor features a fast response time, and was also selective enough to be employed in different biosamples. The signal-off sensor responded sensitively to MAMP with LODs of 30 nM, 50 nM, 20 nM in undiluted serum, urine and 50% saliva, respectively, which were much lower than the clinical concentration threshold. The sensor had no response to other illicit drugs, such as cocaine, ketamine and morphine, verifying the good specificity. This strategy will potentially serve as a rapid tool for illicit drug screening in biofluids, such as preliminary screening of drugged driving.

CRediT authorship contribution statement

Yu Xie: Methodology, Formal analysis, Investigation, Data curation, Writing – original draft. **Shenghong Wu:** Validation. **Zhimin Chen:** Visualization, Investigation. **Jinzhi Jiang:** Project administration. **Jianjun Sun:** Conceptualization, Methodology, Resources.

Declaration of competing interest

The authors declare that they have no known competing financial interests or personal relationships that could have appeared to influence the work reported in this paper.

Acknowledgments

The authors are thankful for the financial support from the National Science Foundation of China (grant no. 21874021), the Natural Science Foundation of Fujian Province, China (grant no. 2019J01205), the Research Fund for International Young Scientists (grant no. 22050410273), and the Open Project Program of the State Key Laboratory of Photocatalysis on Energy and Environment (grant no. SKLPEE-202020). The authors gratefully acknowledge the supporting of Xia-men Pushi nanotechnology Co., Ltd (Fujian, China). Many thanks to Prof. Yi Xiao (North Carolina State University) for the advice and experimental protocol about the fabrication of EAB sensors at early stages.

References

[1] K. Mao, Z. Yang, J. Li, X. Zhou, X. Li, J. Hu, A novel colorimetric biosensor based on non-aggregated Au@Ag core-shell nanoparticles for methamphetamine and cocaine detection, Talanta 175 (2017) 338–346.
[2] T.J. Dickerson, N. Yamamoto, D.I. Ruiz, K.D. Janda, Immunological consequences of methamphetamine protein glycation, J. Am. Chem. Soc. 126 (2004) 11446.
[3] K. Mao, Z. Yang, P. Du, Z. Xu, Z. Wang, X. Li, G-quadruplex–hemin DNAzyme molecular beacon probe for the detection of methamphetamine, RSC Adv 6 (2016) 62754–62759.
[4] K. Mao, Z. Yang, H. Zhang, X. Li, J.M. Cooper, Paper-based nanosensors to evaluate community-wide illicit drug use for wastewater-based epidemiology, Water Res 189 (2021) 116559.
[5] C.L. Winek, W.W. Wahba, T.W. Balzer, Drug and chemical blood-level data 2001, Forensic Sci. Int. 122 (2001) 107–123.
[6] M. Schulz, A. Schmoldt, H. Andresen-Streichert, S. Iwersen-Bergmann, Revisited: therapeutic and toxic blood concentrations of more than 1100 drugs and other xenobiotics, Crit. Care 24 (2020) 195.
[7] R. Dong, S. Weng, L. Yang, J. Liu, Detection and direct readout of drugs in human urine using dynamic surface-enhanced Raman spectroscopy and support vector machines, Anal. Chem. 87 (2015) 2937–2944.
[8] P. Mura, B. Brunet, M.-H. Ghysel-Laporte, J.-P. Goullé, Conduite automobile et amphétamines dans le sang-bases bibliographiques pour un consensus de la Société française de toxicologie analytique, Toxicol. Anal. Clin. 27 (2015) 142–152.
[9] M. Peat, A.E. Davis, Drug Abuse Handbook, CRC Press, Boca Raton, 1998.
[10] A.L. Ciesielski, M.K. Green, J.R. Wagner, Characterization of One Pot methamphetamine laboratories using GC-MS and LC-MS/MS, Forensic Chem 19 (2020), 100244.
[11] B. Subedi, K. Kannan, Mass loading and removal of select illicit drugs in two wastewater treatment plants in New York state and estimation of illicit drug usage in communities through wastewater analysis, Environ. Sci. Technol. 48 (2014) 6661–6670.
[12] F. Cao, J. Xu, S. Yan, X. Yuan, F. Yang, L. Hou, L. Zhao, L. Zeng, W. Liu, L. Zhu, A surface plasmon resonance-based inhibition immunoassay for forensic determination of methamphetamine in human serum, Forensic Chem. 8 (2018) 21–27.
[13] J. Wang, W. Yao, F. Meng, P. Wang, Y. Wu, B. Wang, A surface plasmon resonance immunoassay for the rapid analysis of methamphetamine in

forensic oral fluid, J. Clin. Lab. Anal. 33 (2019), e22993.
[14] C. Andreou, M.R. Hoonejani, M.R. Barmi, M. Moskovits, C.D. Meinhart, Rapid detection of drugs of abuse in saliva using surface enhanced Raman spectroscopy and microfluidics, ACS Nano 7 (2013) 7157–7164.
[15] Z. Han, H. Liu, J. Meng, L. Yang, J. Liu, J. Liu, Portable kit for identification and detection of drugs in human urine using surface-enhanced Raman spectroscopy, Anal. Chem. 87 (2015) 9500–9506.
[16] M.L. Ochoa, P.B. Harrington, Detection of methamphetamine in the presence of nicotine using in situ chemical derivatization and ion mobility spectrometry, Anal. Chem. 76 (2004) 985–991.
[17] R. Wang, X. Qi, S. Liu, L. Zhao, L. Lu, Y. Deng, Ionic liquid-based fluorescence sensing paper: rapid, ultrasensitive, and in-site detection of methamphetamine in human urine, RSC Adv 6 (2016) 52372–52376.
[18] M. Ebrahimi, M. Johari-Ahar, H. Hamzeiy, J. Barar, O. Mashinchian, Y. Omidi, Electrochemical impedance spectroscopic sensing of methamphetamine by a specific aptamer, Bioimpacts 2 (2012) 91.
[19] Y. Zhao, Y. Xie, Q. Zhou, P. Wang, Y. Chang, C. Lin, Automatic sensing setup for methamphetamine based on the reactional wettability variation strategy, ACS Omega 6 (2021) 2045–2051.
[20] J.S. Swensen, Y. Xiao, B.S. Ferguson, A.A. Lubin, H.T. Soh, Continuous, real-time monitoring of cocaine in undiluted blood serum via a microfluidic, electrochemical aptamer-based sensor, J. Am. Chem. Soc. 131 (2009) 4262.
[21] A. Idili, C. Parolo, R. Alvarez-Diduk, A. Merkoci, Rapid and efficient detection of the SARS-CoV-2 spike protein using an electrochemical aptamer-based sensor, ACS Sens. 6 (2021) 3093–3101.
[22] M.A. Pellitero, S.D. Curtis, N. Arroyo-Curras, Interrogation of electrochemical aptamer-based sensors via peak-to-peak separation in cyclic voltammetry improves the temporal stability and batch-to-batch variability in biological fluids, ACS Sens. 6 (2021) 1199–1207.
[23] A.M. Downs, J. Gerson, K.L. Ploense, K.W. Plaxco, P. Dauphin-Ducharme, Subsecond-Resolved molecular measurements using electrochemical phase interrogation of aptamer-based sensors, Anal. Chem. 92 (2020) 14063–14068.
[24] C.Q. Vu, P. Rotkrua, Y. Tantirungrotechai, B. Soontornworajit, Oligonucleotide hybridization combined with competitive antibody binding for the truncation of a high-affinity aptamer, ACS Comb. Sci. 19 (2017) 609–617.
[25] S. Gao, X. Zheng, Y. Tang, Y. Cheng, X. Hu, J. Wu, Development of a fluorescently labeled aptamer structure-switching assay for sensitive and rapid detection of gliotoxin, Anal. Chem. 91 (2019) 1610–1618.
[26] J. He, J. Wang, M. Zhang, G. Shi, Selection of a structure-switching aptamer for the specific methotrexate detection, ACS Sens. 6 (2021) 2436–2441.
[27] M. Ebrahimi, H. Hamzeiy, J. Barar, A. Barzegari, Y. Omidi, Systematic evolution of ligands by exponential enrichment selection of specific aptamer for sensing of methamphetamine, Sens. Lett. 11 (2013) 566–570.
[28] C. Gu, Y. Xiang, H. Guo, H. Shi, Label-free fluorescence detection of melamine with a truncated aptamer, Analyst 141 (2016) 4511–4517.
[29] L.R. Schoukroun-Barnes, F.C. Macazo, B. Gutierrez, J. Lottermoser, J. Liu, R.J. White, Reagentless, structure-switching, electrochemical aptamer-based sensors, Annu. Rev. Anal. Chem. 9 (2016) 163–181.
[30] Analytical Methods Committee, Recommendations for the definition, estimation and use of the detection limit, Analyst 112 (1987) 199–204.
[31] A. Idili, C. Parolo, G. Ortega, K.W. Plaxco, Calibration-Free measurement of phenylalanine levels in the blood using an electrochemical aptamer-based sensor suitable for point-of-care applications, ACS Sens. 4 (2019) 3227–3233.
[32] A. Idili, N. Arroyo-Curras, K.L. Ploense, A.T. Csordas, M. Kuwahara, T.E. Kippin, K.W. Plaxco, Seconds-resolved pharmacokinetic measurements of the chemotherapeutic irinotecan in situ in the living body, Chem. Sci. 10 (2019) 8164–8170.
[33] P.H. Lin, S.J. Tong, S.R. Louis, Y. Chang, W.Y. Chen, Thermodynamic basis of chiral recognition in a DNA aptamer, Phys. Chem. Chem. Phys. 11 (2009) 9744–9750.
[34] Y. Jiang, W. Ma, W. Ji, H. Wei, L. Mao, Aptamer superstructure-based electrochemical biosensor for sensitive detection of ATP in rat brain with in vivo microdialysis, Analyst 144 (2019) 1711–1717.
[35] S. Xu, B. Dai, W. Zhao, L. Jiang, H. Huang, Electrochemical detection of β-lactoglobulin based on a highly selective DNA aptamer and flower-like Au@$BiVO_4$ microspheres, Anal. Chim. Acta 1120 (2020) 1–10.
[36] M.A. Nameghi, N.M. Danesh, M. Ramezani, M. Alibolandi, K. Abnous, S.M. Taghdisi, An ultrasensitive electrochemical sensor for 17β-estradiol using split aptamers, Anal. Chim. Acta 1065 (2019) 107–112.
[37] L. Han, P. Liu, V.A. Petrenko, A. Liu, A label-free electrochemical impedance cytosensor based on specific peptide-fused phage selected from landscape phage library, Sci. Rep. 6 (2016), 22199.
[38] M. Bacchu, M. Ali, S. Das, S. Akter, H. Sakamoto, S.-I. Suye, M. Rahman, K. Campbell, M. Khan, A DNA functionalized advanced electrochemical biosensor for identification of the foodborne pathogen Salmonella enterica serovar Typhi in real samples, Anal. Chim. Acta (2021), 339332.
[39] Q. Xiao, J. Li, X. Jin, Y. Liu, S. Huang, Ultrasensitive electrochemical microRNA-21 biosensor coupling with carboxylate-reduced graphene oxide-based signal-enhancing and duplex-specific nuclease-assisted target recycling, Sensor. Actuator. B Chem. 297 (2019), 126740.
[40] Y. Liu, N. Tuleouva, E. Ramanculov, A. Revzin, Aptamer-based electrochemical biosensor for interferon gamma detection, Anal. Chem. 82 (2010) 8131–8136.
[41] R.J. White, K.W. Plaxco, Exploiting binding-induced changes in probe flexibility for the optimization of electrochemical biosensors, Anal. Chem. 82 (2010) 73–76.
[42] C. Fan, K.W. Plaxco, A.J. Heeger, Electrochemical interrogation of conformational changes as a reagentless method for the sequence-specific detection of DNA, Proc. Natl. Acad. Sci. U.S.A. 100 (2003) 9134–9137.
[43] H. Li, S. Li, J. Dai, C. Li, M. Zhu, H. Li, X. Lou, F. Xia, K.W. Plaxco, High frequency, calibration-free molecular measurements in situ in the living body, Chem. Sci. 10 (2019) 10843–10848.
[44] A.H. Oghli, E. Alipour, M. Asadzadeh, Development of a novel voltammetric sensor for the determination of methamphetamine in biological samples on the pretreated pencil graphite electrode, RSC Adv 5 (2015) 9674–9682.
[45] B. Demir, T. Yilmaz, E. Guler, Z.P. Gumus, H. Akbulut, E. Aldemir, H. Coskunol, D.G. Colak, I. Cianga, S. Yamada, S. Timur, T. Endo, Y. Yagci, Polypeptide with electroactive endgroups as sensing platform for the abused drug 'methamphetamine' by bioelectrochemical method, Talanta 161 (2016) 789–796.
[46] B. Rafiee, A.R. Fakhari, M. Ghaffarzadeh, Impedimetric and stripping voltammetric determination of methamphetamine at gold nanoparticles-multiwalled carbon nanotubes modified screen printed electrode, Sensor. Actuator. B Chem. 218 (2015) 271–279.
[47] C.-H. Yeh, W.-T. Wang, P.-L. Shen, Y.-C. Lin, A developed competitive immunoassay based on impedance measurements for methamphetamine detection, Microfluid. Nanofluidics 13 (2012) 319–329.
[48] Z. Cai, Z. Lin, X. Chen, T. Jia, P. Yu, X. Chen, Electrochemiluminescence detection of methamphetamine based on a $Ru(bpy)_3^{2+}$-doped silica nanoparticles/Nafion composite film modified electrode, Luminescence 25 (2010) 367–372.
[49] M. Masteri-Farahani, F. Askari, Design and photophysical insights on graphene quantum dots for use as nanosensor in differentiating methamphetamine and morphine in solution, Spectrochim. Acta Mol. Biomol. Spectrosc. 206 (2019) 448–453.
[50] S. Mandani, B. Rezaei, A.A. Ensafi, Sensitive imprinted optical sensor based on mesoporous structure and green nanoparticles for the detection of methamphetamine in plasma and urine, Spectrochim. Acta Mol. Biomol. Spectrosc. 231 (2020) 118077.
[51] T.-C. Chang, C.-Y. Chiang, M.-H. Lin, I.K. Chen, L.-K. Chau, D.-S. Hsu, S.-S. Shieh, C.-J. Kuo, S.-C. Wang, Y.-f. Chen, Fiber optic particle plasmon resonance immunosensor for rapid and sensitive detection of methamphetamine based on competitive inhibition, Microchem. J. 157 (2020), 105026.
[52] Q. Shi, Y. Shi, Y. Pan, Z. Yue, H. Zhang, C. Yi, Colorimetric and bare eye determination of urinary methylamphetamine based on the use of aptamers and the salt-induced aggregation of unmodified gold nanoparticles, Microchim. Acta 182 (2014) 505–511.